Report

Cell Reports

Crystal Structure and Activity of the Endoribonuclease Domain of the piRNA Pathway Factor Maelstrom

Graphical Abstract

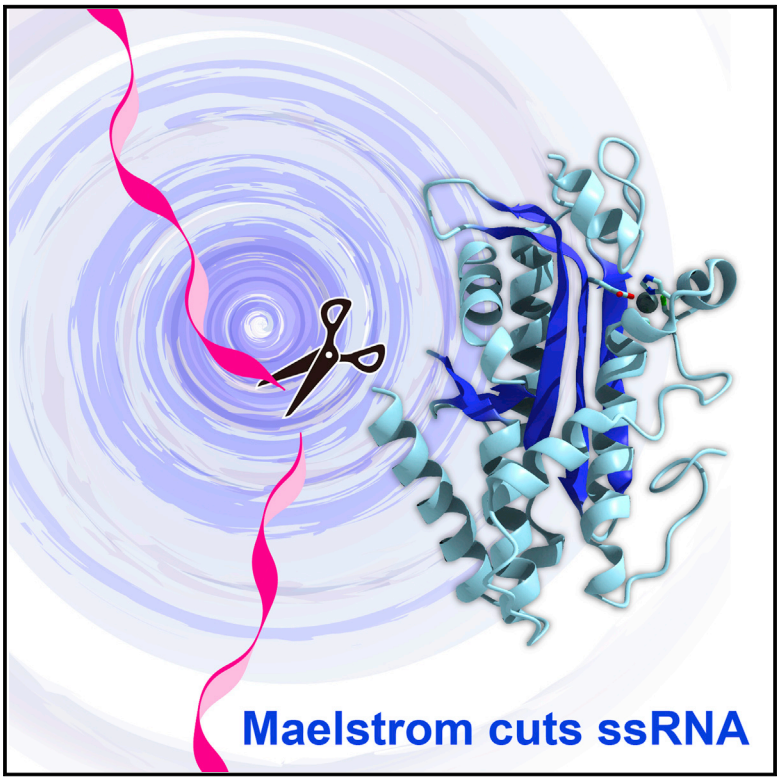

Authors

Naoki Matsumoto, Kaoru Sato, ..., Mikiko C. Siomi, Osamu Nureki

Correspondence

siomim@bs.s.u-tokyo.ac.jp (M.C.S.), nureki@bs.s.u-tokyo.ac.jp (O.N.)

In Brief

Maelstrom (Mael) is essential for transposon silencing in the piRNA pathway. Using structural and functional approaches, Matsumoto et al. show that Mael lacks the canonical nuclease active-site structure but exhibits single-stranded RNA cleavage activity, unrelated to transposon silencing, in flies.

Highlights

- Crystal structure of the MAEL domain in *Drosophila* Maelstrom is determined
- The MAEL domain has an RNase H-like fold but lacks canonical catalytic residues
- The MAEL domain shows single-strand-specific endoribonuclease activity
- The ssRNase activity of Mael is unrelated to transposon silencing

Accession Numbers

4YBG
LC032360

Matsumoto et al., 2015, Cell Reports *11*, 366–375
April 21, 2015
http://dx.doi.org/10.1016/j.celrep.2015.03.030

CellPress

OPEN ACCESS
CellPress

Cell Reports
Report

Crystal Structure and Activity of the Endoribonuclease Domain of the piRNA Pathway Factor Maelstrom

Naoki Matsumoto,[1,5] Kaoru Sato,[1,5] Hiroshi Nishimasu,[1,2,5] Yurika Namba,[1] Kana Miyakubi,[1] Naoshi Dohmae,[3] Ryuichiro Ishitani,[1] Haruhiko Siomi,[4] Mikiko C. Siomi,[1,*] and Osamu Nureki[1,*]
[1]Department of Biological Sciences, Graduate School of Science, The University of Tokyo, Tokyo 113-0032, Japan
[2]JST, PRESTO, Tokyo 113-0032, Japan
[3]Biomolecular Characterization Team and CREST/JST, RIKEN, 2-1 Hirosawa, Wako, Saitama 351-0198, Japan
[4]Department of Molecular Biology, Keio University School of Medicine, Tokyo 160-8582, Japan
[5]Co-first author
*Correspondence: siomim@bs.s.u-tokyo.ac.jp (M.C.S.), nureki@bs.s.u-tokyo.ac.jp (O.N.)
http://dx.doi.org/10.1016/j.celrep.2015.03.030

SUMMARY

PIWI-interacting RNAs (piRNAs) protect the genome from transposons in animal gonads. Maelstrom (Mael) is an evolutionarily conserved protein, composed of a high-mobility group (HMG) domain and a MAEL domain, and is essential for piRNA-mediated transcriptional transposon silencing in various species, such as *Drosophila* and mice. However, its structure and biochemical function have remained elusive. Here, we report the crystal structure of the MAEL domain from *Drosophila melanogaster* Mael, at 1.6 Å resolution. The structure reveals that the MAEL domain has an RNase H-like fold but lacks canonical catalytic residues conserved among RNase H-like superfamily nucleases. Our biochemical analyses reveal that the MAEL domain exhibits single-stranded RNA (ssRNA)-specific endonuclease activity. Our cell-based analyses further indicate that ssRNA cleavage activity appears dispensable for piRNA-mediated transcriptional transposon silencing in *Drosophila*. Our findings provide clues toward understanding the multiple roles of Mael in the piRNA pathway.

INTRODUCTION

Small RNA-based defense systems repress the aberrant expression of transposable elements (TEs) and thus maintain genome integrity in animal gonads (Malone and Hannon, 2009; Siomi et al., 2011). The germline-specific PIWI clade of Argonaute family proteins and the 23- to 30-nt noncoding PIWI-interacting RNAs (piRNAs) are the core of this defense system. PIWI proteins bind piRNAs to form piRNA-induced silencing complexes (piRISCs), which silence their complementary target TEs at the transcriptional or posttranscriptional level (Malone and Hannon, 2009; Siomi et al., 2011; Ishizu et al., 2012; Luteijn and Ketting, 2013). The *Drosophila* genome encodes three PIWI proteins: Piwi, Aubergine (Aub), and Argonaute3 (AGO3). The *Drosophila* ovary consists of two types of cells, somatic cells such as follicle cells, and germ cells such as nurse cells and oocytes. Piwi is localized in the nucleus in both somatic and germ cells, where it participates in the primary piRNA pathway (Czech et al., 2013; Handler et al., 2013; Olivieri et al., 2010). In contrast, Aub and AGO3 are enriched in cytoplasmic perinuclear granules called nuage in germ cells, where they participate in secondary piRNA biogenesis (Brennecke et al., 2007; Gunawardane et al., 2007; Li et al., 2009; Malone et al., 2009). In the primary piRNA pathway in *Drosophila* ovarian somatic cells, single-stranded, long piRNA precursors are transcribed from discrete genomic loci, called piRNA clusters, and are processed into mature piRNAs by the single-strand-specific endoribonuclease Zucchini (Zuc) (Ipsaro et al., 2012; Nishimasu et al., 2012). The primary piRNAs are loaded into Piwi at cytoplasmic perinuclear Yb bodies (Saito et al., 2010). piRISC then enters the nucleus and promotes repressive histone H3 lysine 9 trimethylation (H3K9me3), thereby silencing target TEs at the transcriptional level (Sienski et al., 2012; Wang and Elgin, 2011; Le Thomas et al., 2013; Rozhkov et al., 2013). In the secondary piRNA biogenesis pathway, Aub and AGO3 reciprocally cleave sense and antisense TE transcripts, respectively (Brennecke et al., 2007; Gunawardane et al., 2007). This feed-forward piRNA amplification loop, called the ping-pong cycle, enables simultaneous secondary piRNA biogenesis and TE silencing.

Maelstrom (Mael) is an evolutionarily conserved protein implicated in the piRNA pathway (Lim and Kai, 2007; Soper et al., 2008; Aravin et al., 2009; Sienski et al., 2012; Castañeda et al., 2014). In somatic cells of the fly ovary, Mael is predominantly localized in the nucleus (Sienski et al., 2012). In contrast, in germ cells of the fly ovary and mouse testis, Mael is localized in both the nucleus and cytoplasmic granules (nuage in flies, piP-bodies or chromatoid bodies in mice) (Findley et al., 2003; Costa et al., 2006; Lim and Kai, 2007; Soper et al., 2008; Aravin et al., 2009; Sato et al., 2011; Castañeda et al., 2014). Mael is also implicated in various biological processes, such as oocyte development and germline stem cell (GSC) differentiation (Clegg

et al., 1997, 2001; Pek et al., 2009, 2012; Sato et al., 2011). Mael is composed of an N-terminal HMG domain and a central MAEL domain, which was predicted to adopt an RNase H-like fold by a bioinformatics analysis (Zhang et al., 2008) (Figures 1A and S1). However, the biochemical function of Mael remains elusive.

In cultured *Drosophila* ovarian somatic cells (OSCs) (Niki et al., 2006; Saito et al., 2009), *mael* knockdown (KD) did not affect piRNA biogenesis but resulted in the derepression of TEs, indicating that Mael is essential for Piwi-mediated TE silencing (Sienski et al., 2012). Intriguingly, *mael* KD only modestly impacted the H3K9me3 patterns at the target heterochromatic loci, suggesting that Mael acts downstream of or in parallel to the Piwi-mediated H3K9me3 modification (Sienski et al., 2012). In addition, Mael has been implicated in piRNA biogenesis in germ cells of the fly ovary and mouse testis (Lim and Kai, 2007; Sienski et al., 2012; Aravin et al., 2009; Castañeda et al., 2014). Despite the crucial role of Mael in the piRNA pathway, the molecular mechanism of Mael/Piwi-mediated TE silencing remains elusive, due to the lack of structural and biochemical information.

In this study, we solved the crystal structure of the MAEL domain of *D. melanogaster* Mael. The structure revealed that the MAEL domain adopts an RNase H-like fold but lacks the canonical catalytic residues conserved among the RNase H-like superfamily of endonucleases and exonucleases. Moreover, our biochemical and biological analyses revealed that the MAEL domain has single-stranded RNA (ssRNA) cleavage activity, which appears dispensable for Mael/Piwi-mediated transcriptional TE silencing in *Drosophila* OSCs. Our findings provide clues toward understanding the multiple functions of Mael in the piRNA pathway.

RESULTS

Crystal Structure of the MAEL Domain from *D. melanogaster* Mael

To gain mechanistic insights into the function of Mael, we attempted to determine the crystal structure of full-length *D. melanogaster* Mael (residues 1–459, referred to as FL-DmMael) but were hampered by its low expression levels in *Escherichia coli*. Limited trypsin proteolysis of FL-DmMael revealed that the MAEL domain (residues 84–333, referred to as DmMAEL) is a well-expressed, stable region suitable for structural analysis (Figure 1A). Furthermore, we found that the substitution of a less-conserved cysteine residue (Cys228) with serine dramatically improved the diffraction quality. X-ray fluorescence spectra of the crystal indicated that DmMAEL binds a zinc ion, consistent with a previous bioinformatics analysis suggesting that a zinc ion is coordinated by the ECHC motif, which is conserved among Mael orthologs (Zhang et al., 2008) (Figures S1 and S2). We determined the crystal structure of DmMAEL (C228S) at 1.6 Å resolution by the single-wavelength anomalous diffraction (SAD) method, using the intrinsic zinc atom (Figure 1B; Table S1). The structure revealed that DmMAEL consists of a twisted five-stranded mixed β sheet surrounded by 13 helices, with a zinc ion coordinated by Glu131, Cys288, His291, and Cys300 in the ECHC motif (Figure 1C).

A Dali search (Holm and Rosenström, 2010) revealed that DmMAEL shares structural similarity with the RNase H-like superfamily of endonucleases and exonucleases (Majorek et al., 2014), especially with the DEDDh family exonucleases, such as a Lassa virus nucleoprotein (LASV NP) (PDB 4GV9) (Jiang et al., 2013). LASV NP is a 3′–5′ exonuclease involved in the suppression of virus-induced interferon production (Martínez-Sobrido et al., 2007; Qi et al., 2010; Hastie et al., 2011; Jiang et al., 2013). Despite their low sequence identity (~13%), DmMAEL shares an RNase H-like fold, consisting of a five-stranded β sheet flanked by α helices on both sides, with LASV NP (Jiang et al., 2013) (root mean square deviation of 2.9 Å for 131 aligned Cα atoms) (Figure 1D). Like DmMAEL, LASV NP contains a zinc ion coordinated by the ECHC motif, consisting of Glu399, Cys506, His509, and Cys529, which may contribute to structural stabilization or substrate binding (Qi et al., 2010; Hastie et al., 2011) (Figures 1E and S3A). In DmMAEL, the bound zinc ion may play at least a structural role, since point mutations of the ECHC motif drastically reduced the solubility of DmMAEL in vitro (data not shown). The DEDDh family exonucleases have a negatively charged catalytic groove formed by five invariant catalytic residues (Asp, Glu, Asp, Asp, and His; DEDDh motif) and cleave double-stranded RNAs (dsRNAs) through a two-metal-ion mechanism (Zuo and Deutscher, 2001). In LASV NP, the catalytic groove is formed by Asp389, Glu391, Asp466, Asp533, and His528 in the DEDDh motif and the highly conserved Ser430, Gln462, and Arg492 residues (Hastie et al., 2012; Jiang et al., 2013) (Figures 1F and S3B). The Asp389, Glu391, Asp466, Asp533, and His528 residues of LASV NP respectively correspond to the Ala114, Asn116, Met218, Met304, and Tyr299 residues of DmMAEL (Figures 1F and S3B). Consequently, the central groove of DmMAEL, which corresponds to the catalytic groove of LASV NP, is not negatively charged (Figure 1G). In addition, the residues in the central groove are not conserved among Mael orthologs (Figures S1 and S2), suggesting that the central groove is less important for the function of Mael. Taken together, the crystal structure of DmMAEL revealed that it adopts an RNase H-like fold but lacks the canonical catalytic residues conserved among RNase H-like superfamily members.

The MAEL Domain Has Single-Strand-Specific Endoribonuclease Activity

To determine whether DmMAEL is a nuclease, we measured the nuclease activity of purified DmMAEL using a 5′ ^{32}P-labeled 40-nt ssRNA (40AS ssRNA) as the substrate. Unexpectedly, DmMAEL cleaved the 40AS ssRNA (Figure 2A). The elution profile of purified DmMAEL correlated closely with that of the single-stranded ribonuclease (ssRNase) activity in gel-filtration chromatography (Figure 2A). Furthermore, DmMAEL cleaved the 40AS ssRNA in a dose- and time-dependent manner (Figures 2B and 2C). These results revealed that DmMAEL is a ssRNase. The ssRNase activity of DmMAEL did not require divalent metal ions, such as Mg^{2+} or Ca^{2+}, and was rather inhibited in their presence (Figure 2D). These results are consistent with our structural finding that DmMAEL shares no catalytic residues with the DEDDh family members, which require divalent metal ions, such as Mg^{2+} and Mn^{2+}, for substrate cleavage (Zuo and Deutscher, 2001). To determine the substrate specificity of

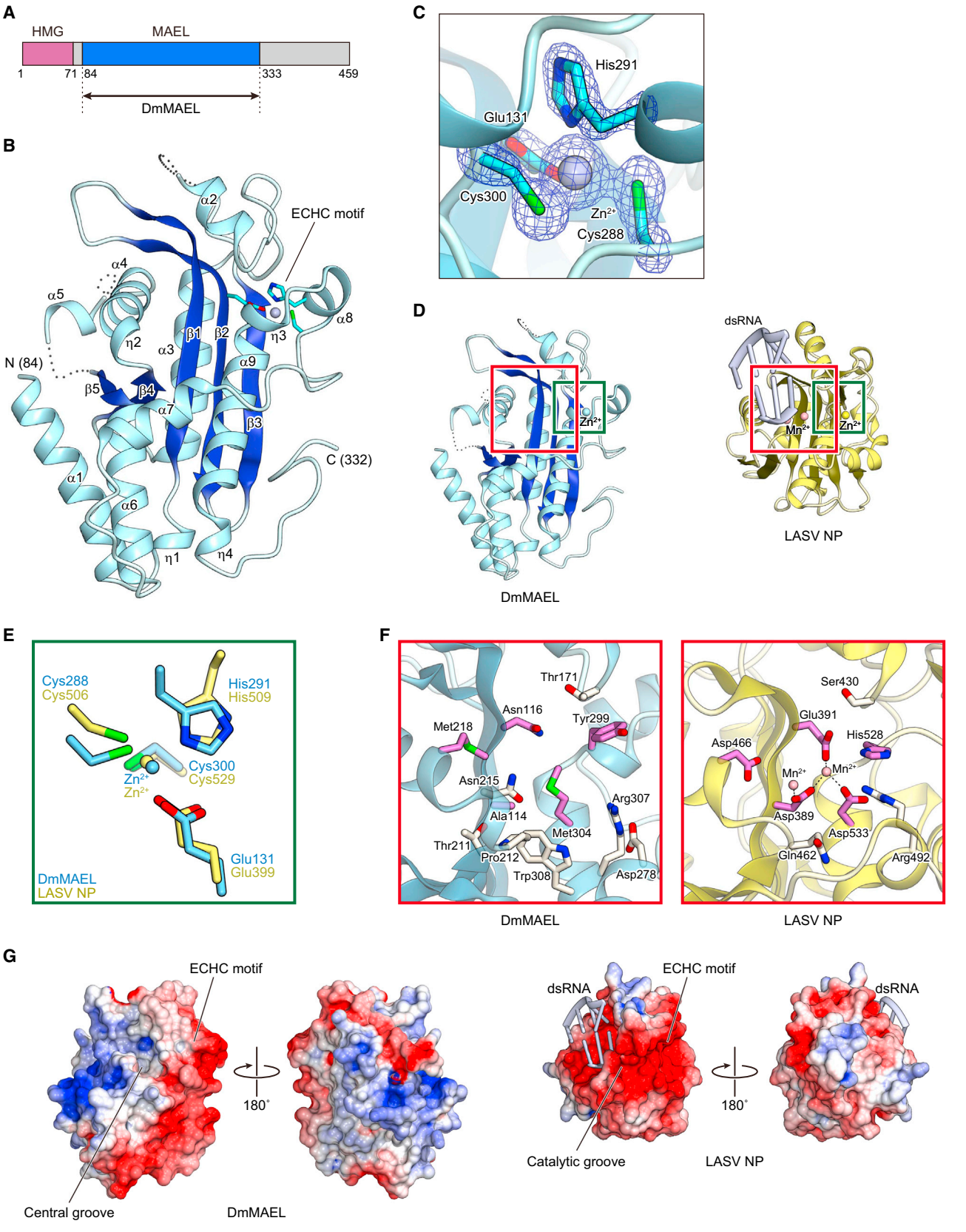

(legend on next page)

DmMAEL, we next measured the cleavage activity toward a series of 5′ ^{32}P-labeled nucleic acid substrates. DmMAEL efficiently cleaved ssRNA, but neither dsRNA nor ssDNA (Figure 2E). DmMAEL cleaved circular 40AS ssRNA, indicating that DmMAEL is an endoribonuclease (Figure 2F). The cleavage pattern of the 40AS ssRNA revealed that DmMAEL preferentially cleaves ssRNA at a guanine residue (especially at successive guanine stretches) (Figure 2E). To exclude the possibility that the 40AS ssRNA adopts a secondary structure that affects the cleavage by DmMAEL, we measured the nuclease activity of DmMAEL toward 15-nt poly(A) RNA substrates with or without guanine residues, which are unlikely to adopt secondary structures. DmMAEL cleaved 15-nt poly(A) containing guanine residues, but not 15-nt poly(A), confirming that DmMAEL cleaves ssRNA at guanine residues (Figure 2G). We next compared the cleavage patterns of the 40AS ssRNA by DmMAEL and RNase T1, an endonuclease that specifically cleaves ssRNA at the 3′ side of guanine residues (Pace et al., 1991). RNase T1 cleaved the 40AS ssRNA evenly at guanine residues (Figure 2H). In contrast, DmMAEL did not efficiently cleave the 40AS ssRNA at 3 nt from the 5′ end (position 1) and 4 nt from the 3′ end (position 6) (Figure 2H). The ssRNase activity of DmMAEL was inhibited in the presence of 25 mM NaCl, whereas that of RNase T1 remained robust in the presence of 100 mM NaCl (Figure 2I). These differences in their enzymatic properties indicated that the RNA cleavage mechanism of DmMAEL is distinct from that of RNase T1. To examine whether the nuclease activity is specific to *D. melanogaster* Mael, we measured the ssRNase activities of the purified MAEL domains from *Bombyx mori* Mael (residues 92–335, referred to as BmMAEL) and *Mus musculus* Mael (residues 83–327, referred to as MmMAEL) (Figure 2J). We found that both BmMAEL and MmMAEL cleave the 40AS ssRNA in similar manners to that of DmMAEL, although the ssRNase activity of MmMAEL was weaker than those of DmMAEL and BmMAEL (Figure 2J). Together, these biochemical data revealed that the MAEL domain is an evolutionarily conserved, single-strand-specific endoribonuclease.

Potential RNA-Binding Residues of the MAEL Domain

Since the MAEL domain lacks the canonical DEDDh motif, we tried to identify the catalytic residues of DmMAEL, based on the sequence conservation among Mael orthologs. However, multiple sequence alignments indicated that only the ECHC motif is solvent accessible and strictly conserved across the Mael orthologs (Figures S1 and S2). Thus, based on the crystal structure of DmMAEL, we prepared 12 DmMAEL mutants, in which the solvent-exposed, hydrophilic residues were individually substituted with alanine (Figure 3A). All of the mutants eluted as a single monodisperse peak from the gel-filtration column (data not shown), confirming their structural integrity. We then examined the ssRNase activities of the purified mutants, using 40AS ssRNA as the substrate (Figure 3B). The K109A, K188A, N192A, and E292A mutants showed ssRNase activities comparable to that of the wild-type DmMAEL, and the K277A mutant showed moderately reduced ssRNase activity (Figure 3B). In contrast, the K140A, K199A, Q289A, D293A, D295A, D314A, and K328A mutants showed markedly reduced ssRNase activities (Figure 3B), indicating that Lys140, Lys199, Gln289, Asp293, Asp295, Asp314, and Lys328 are involved in the ssRNase activity. Although DmMAEL, BmMAEL, and MmMAEL cleaved ssRNA in a similar manner (Figure 2J), these residues (except for Asp295) are not conserved among the Mael orthologs (Figure S1). Moreover, these mutations reduced, but did not abolish, the ssRNase activity (Figure 3B), suggesting that these residues are involved in ssRNA binding, but not in catalysis. The positively charged residues, Lys140, Lys199, and Lys328, would interact with the negatively charged phosphate backbone of the ssRNA substrates. These residues are located on the opposite side of the central groove, which is equivalent to the catalytic groove of LASV NP (Figures 3C and 3D). To examine whether the central groove is involved in the ssRNase activity, we tried to prepare four additional DmMAEL mutants (N116A, M218A, Y299A, and M304A), in which the residues corresponding to the DEDDh motif were individually substituted with alanine. These four mutants were not expressed in *E. coli* as soluble proteins (data not shown), suggesting that these residues within the central groove contribute to structural integrity. In addition, the C228S mutant used for our structural analysis exhibited the ssRNase activity (Figure 3B), indicating that the C228S mutation does not have considerable impact on the structure and function of DmMAEL.

Since both DmMAEL and RNase T1 preferentially cleave ssRNA at guanine residues, we attempted to detect the structural similarity between them. RNase T1 cleaves ssRNA through a metal-ion-independent mechanism, in which a conserved histidine serves as a catalytic residue (Pace et al., 1991). Since His329 of DmMAEL is the only histidine residue conserved among DmMAEL, BmMAEL, and MmMAEL (Figure S1), we examined the RNase activity of the DmMAEL H329A mutant (Figure 3A). The H329A mutant retained

Figure 1. Crystal Structure of DmMAEL

(A) Domain structure of *D. melanogaster* Mael.

(B) Overall structure of DmMAEL. The zinc ion is shown as a gray sphere. Disordered regions (residues 156–162, 228–229, and 236–237) are shown as dashed lines.

(C) Close-up view of the ECHC motif. An $F_O - F_C$ simulated annealing omit map contoured at 3.5σ is shown as a blue mesh.

(D) Structures of DmMAEL (left) and LASV NP in complex with dsRNA (PDB ID 4GV9) (right). The zinc ions are shown as light blue and yellow spheres in DmMAEL and LASV NP, respectively. The manganese ions are shown as pink spheres. The ECHC motif and the central groove are indicated by green and red boxes, respectively.

(E) Superimposition of the ECHC motifs of DmMAEL and LASV NP.

(F) Central grooves of DmMAEL (left) and LASV NP (right). In LASV NP, the DEDDh-motif and RNA-binding residues are shown as magenta and white sticks, respectively. The bound manganese ions are shown as pink spheres, and the bound dsRNA is omitted for clarity. In DmMAEL, the equivalent residues in the central groove are shown in the same color code. Coordination bonds are shown as dashed lines.

(G) Electrostatic surface potentials of DmMAEL and LASV NP (contoured from −5 kT/e [red] to +5 kT/e [blue]).

See also Figures S1–S3 and Table S1.

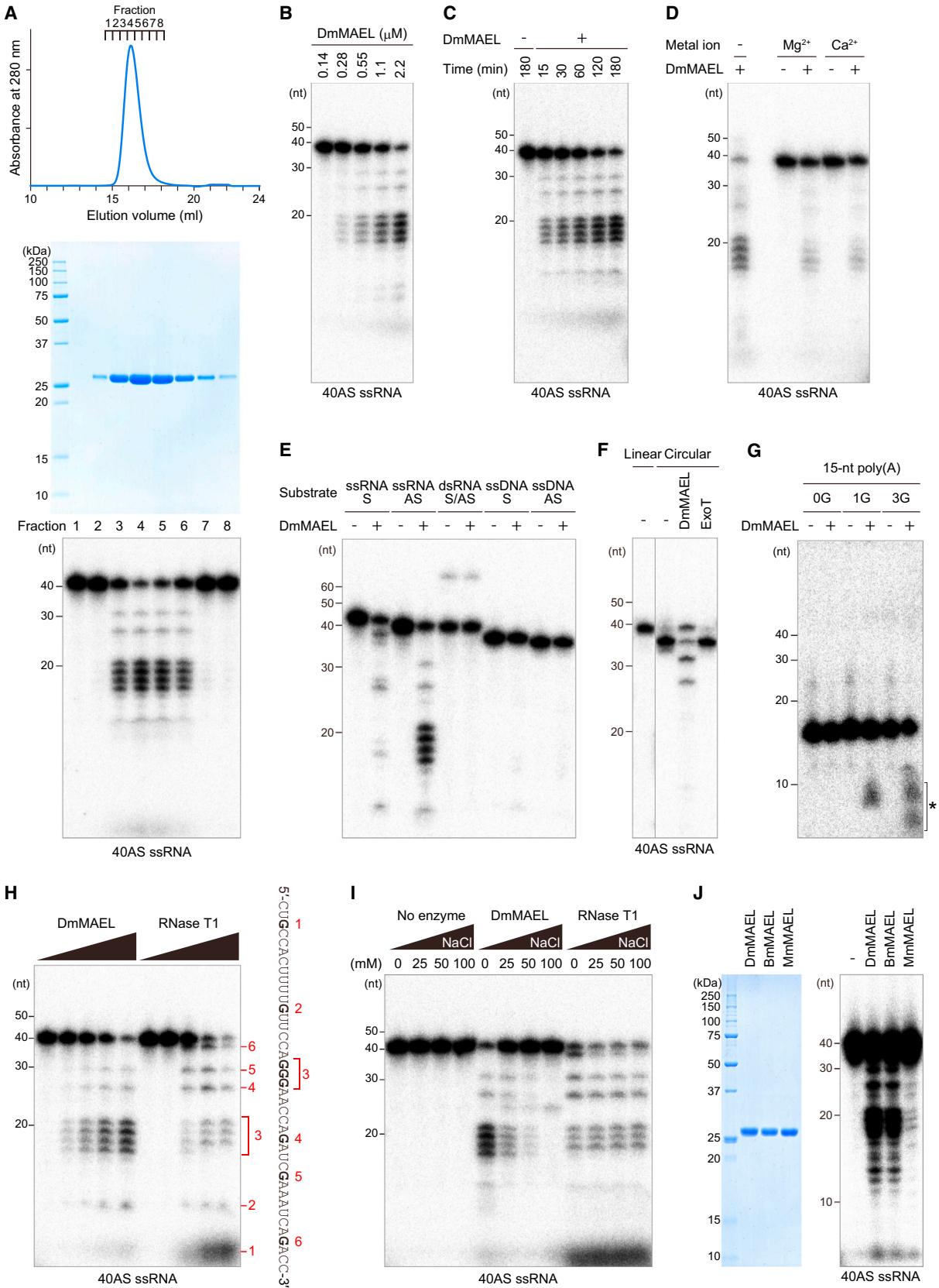

(legend on next page)

the ssRNase activity, indicating that His329 is not involved in ssRNA cleavage (Figure 3B). Thus, despite our numerous attempts, the RNA cleavage mechanism remains to be elucidated. Nonetheless, our mutational analyses support the notion that Mael does not share an active site with either RNase T1 or the DEDDh family members.

The ssRNase Activity of Mael Appears Dispensable for Piwi/Mael-Mediated TE Silencing in *Drosophila* OSCs

To examine the contribution of the MAEL domain to Piwi/Mael-mediated TE silencing, we overexpressed DmMAEL, FL-DmMael, the four ECHC-motif single mutants (E131A, C288A, H291A, and C300A) of FL-DmMael, the ECHC-motif quadruple mutants (E131A/C288A/H291A/C300A) of FL-DmMael, and DmMAEL in *mael*-depleted OSCs and then monitored the expression levels of TEs by qRT-PCR. FL-DmMael and DmMAEL rescued the derepression of a variety of somatic TEs (*mdg1*, *297*, *blood*, *Tabor*, *gypsy*, and *ZAM*) (Figures 4A, 4B, and S4A), indicating that the MAEL domain plays a central role in Piwi/Mael-mediated TE silencing in *Drosophila* OSCs, consistent with a previous report (Sienski et al., 2012). All of the ECHC-motif mutants of FL-DmMael and DmMAEL failed to rescue TE derepression (Figures 4A and S4B), highlighting the functional significance of the ECHC motif for Piwi/Mael-mediated TE silencing.

To examine whether the ssRNase activity of DmMAEL is involved in Piwi/Mael-mediated TE silencing, we next overexpressed the seven ssRNase-deficient DmMAEL mutants (K140A, K199A, Q289A, D293A, D295A, D314A, and K328A) in *mael*-depleted OSCs and then monitored the levels of TE derepression. Like wild-type DmMAEL, all seven of the ssRNase-deficient mutants rescued TE derepression (Figures 4A and S4C). Since the ECHC-motif mutants of DmMAEL were not expressed in *E. coli* as soluble proteins, we could not examine their ssRNase activities in vitro. Overall, these results suggested that the ssRNA cleavage activity of Mael appears dispensable for Piwi/Mael-mediated TE silencing in *Drosophila* OSCs.

DISCUSSION

The present crystal structure revealed that DmMAEL adopts an RNase H-like fold but does not share catalytic residues with the RNase H-like superfamily members. Unexpectedly, our biochemical analyses revealed that DmMAEL has ssRNase activity. We further showed that BmMAEL and MmMAEL also have the ssRNase activities, and we identified seven potential ssRNA-binding residues of DmMAEL. These results strongly support our surprising finding that the MAEL domain possesses the ssRNase activity, although it lacks the canonical active site conserved across the RNase H-like superfamily nucleases.

Previous studies showed that Mael participates in piRNA biogenesis in germ cells of the fly ovary and mouse testis (Lim and Kai, 2007; Sienski et al., 2012; Aravin et al., 2009; Castañeda et al., 2014). In the adult mouse testis, a ribonucleoprotein complex comprising Mael, the PIWI protein MIWI, and the Tudor-domain-containing protein TDRD6 is involved in the processing of precursor transcripts into mature pachytene piRNAs, a class of mammalian piRNAs (Castañeda et al., 2014). Notably, the nuclease activity of MIWI is not required for piRNA biogenesis (Reuter et al., 2011), and the ribonucleoprotein complex lacks a potential nuclease (Castañeda et al., 2014), suggesting that Mael may be responsible for the processing of pachytene piRNA precursors in adult mouse testis. This model is consistent with our finding that MmMAEL exhibits the ssRNase activity. Together, these observations suggested that the ssRNase activity of Mael is involved in the processing of piRNA precursors in mice.

A previous study showed that the MAEL domain plays a central role in Piwi/Mael-mediated TE silencing in *Drosophila* OSCs (Sienski et al., 2012). In OSCs, the *mael* KD has mild effects on the establishment of H3K9me3 but increases RNA polymerase II occupancy at target heterochromatic loci, thereby resulting in the derepression of TEs (Sienski et al., 2012). These observations indicated that Mael acts downstream of or in parallel to the H3K9me3 modification event. A large-scale genetic screen further indicated that, in addition to Piwi and Mael, the zinc finger domain-containing protein Gtsf1 (Dönertas et al., 2013; Ohtani et al., 2013) and several chromatin-associated factors, such as the histone deacetylase HDAC3 and the histone chaperone Asf1, are involved in the *Drosophila* somatic piRNA pathway (Handler et al., 2013; Muerdter et al., 2013). Consistent with the previous report (Sienski et al., 2012), our cell-based analysis indicated that the MAEL domain is involved in TE silencing in *Drosophila* OSCs. Our mutational analysis

Figure 2. ssRNA-Cleavage Activity of the MAEL Domain

(A) ssRNase activity of DmMAEL. The gel-filtration chromatography elution profile of DmMAEL (top). SDS-PAGE analysis (middle) and ssRNase activity of fractions 1–8 (bottom). Each fraction (1 μl) was incubated with the 40AS ssRNA and then analyzed by 15% denaturing PAGE.

(B) Dose dependency of the DmMAEL ssRNase activity. DmMAEL (0.14–2.2 μM) was incubated with the 40AS ssRNA at 26°C for 3 hr.

(C) Time dependency of the DmMAEL ssRNase activity. DmMAEL (2.2 μM) was incubated with the 40AS ssRNA at 26°C for 15–180 min.

(D) Effect of divalent cations on the DmMAEL ssRNase activity.

(E) Substrate specificities of DmMAEL. "S" and "AS" indicate the sense and antisense strands of dsRNA, respectively.

(F) ssRNase activity of DmMAEL toward linear and circular 40AS ssRNA. Exonuclease T (ExoT) was used as a control.

(G) ssRNase activity of DmMAEL toward 15-nt poly(A) ssRNA with and without guanine residues. The asterisk indicates the cleavage products.

(H) Comparison of the ssRNase activities of DmMAEL with RNase T1. DmMAEL (0.14–2.2 μM) or RNase T1 (0.5–10 units) was incubated with the 40AS ssRNA at 26°C for 3 hr. The nucleotide sequence of the substrate 40AS ssRNA is shown on the right of the gel, with guanine residues highlighted in bold. The predicted cleavage sites are indicated by red numbers.

(I) Comparison of the ssRNase activities of DmMAEL and RNase T1 in the presence of NaCl.

(J) ssRNase activities of DmMAEL, BmMAEL, and MmMAEL. SDS-PAGE analysis (left) and ssRNase activities (right) of purified DmMAEL, BmMAEL, and MmMAEL.

See also Table S2.

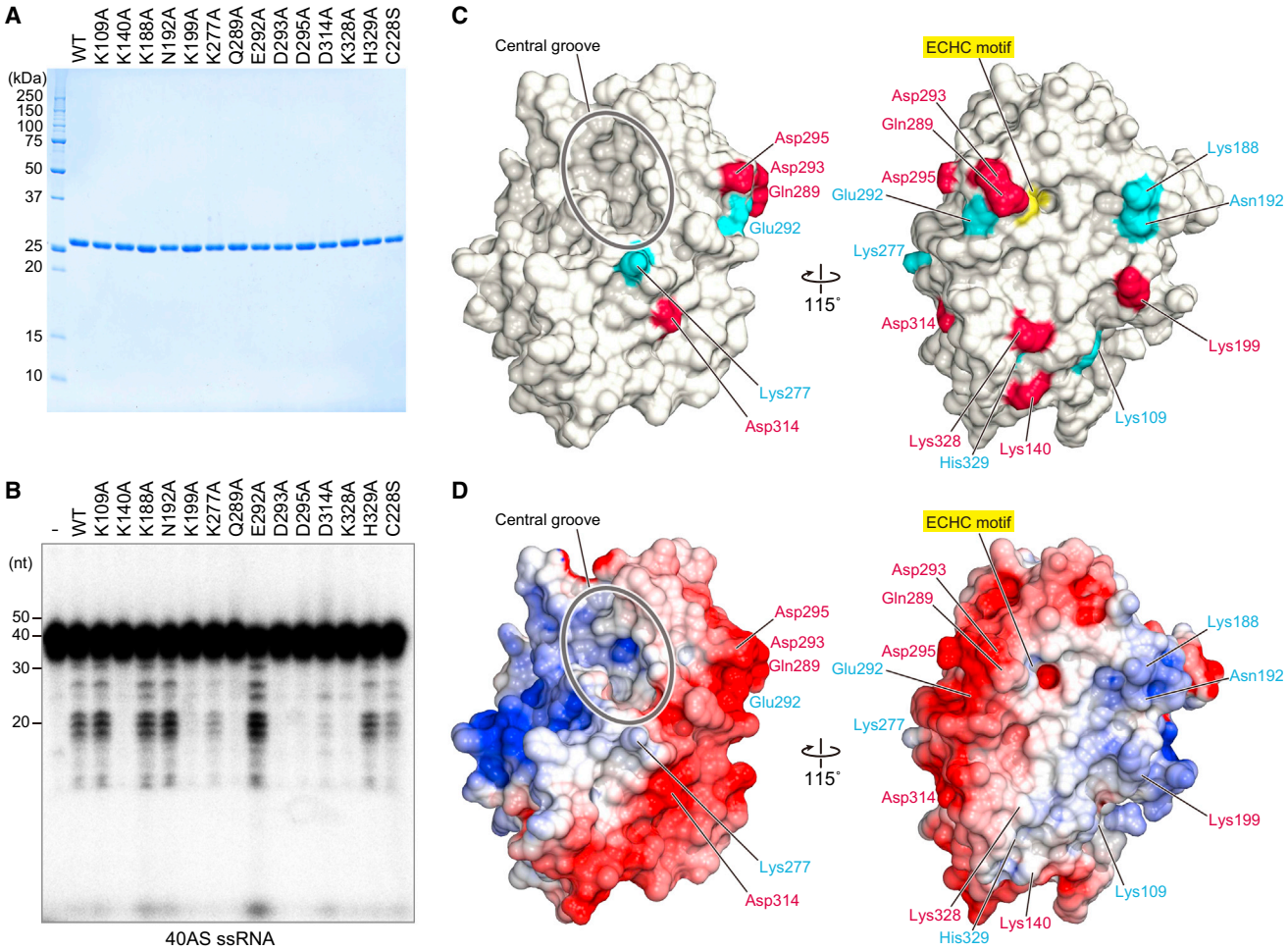

Figure 3. Potential ssRNA-Binding Residues of DmMAEL

(A) Purified wild-type and mutants of DmMAEL. WT, wild-type.

(B) ssRNase activities of purified wild-type and mutants of DmMAEL. The ssRNase activities were measured using the 40AS ssRNA as the substrate.

(C) Structural mapping of the ssRNase-deficient mutations. Residues involved in ssRNA cleavage are colored red, whereas residues not involved in ssRNA cleavage are colored cyan. The ECHC motif is colored yellow. The central groove is indicated by a gray circle.

(D) Electrostatic surface potentials of DmMAEL, viewed from the same direction as in (C) (contoured from −5 kT/e [red] to +5 kT/e [blue]).

further suggested that the ssRNase activity of the MAEL domain appears dispensable for TE silencing. Thus, we propose that Mael interacts with other piRNA factors via the MAEL domain and thereby participates in TE silencing in *Drosophila* OSCs.

A previous bioinformatics analysis suggested that the MAEL domain evolved from a DEDDh exonuclease by switching the catalytic residues from the DEDDh motif to the ECHC motif and that the MAEL domain may possess the nuclease activity (Zhang et al., 2008). Consistent with this, our structural and biochemical data revealed that the MAEL domain lacks the DEDDh motif but shows ssRNase activity. Given that the ECHC motif is strictly conserved among Mael orthologs (Figures S1 and S2), the ECHC motif may play a catalytic role in addition to a structural role. This idea is supported by the observation that Asp295 of DmMAEL, which is highly conserved and located close to the ECHC motif, is involved in the ssRNase activity.

If the ECHC motif participates in catalysis, then it is possible that the ssRNase activity of Mael is involved in TE silencing in *Drosophila* OSCs, since the ECHC-motif mutants failed to rescue TE derepression in our cell-based rescue experiments. All of the ssRNase-deficient DmMAEL mutants we examined in our cell-based assays retained slight ssRNase activities in vitro, which might be sufficient for TE silencing when overexpressed in OSCs. Indeed, in our previous study on Zuc, an endoribonuclease implicated in primary piRNA biogenesis, TE derepression was not rescued by the overexpression of the catalytically inactive Zuc mutant but was efficiently rescued by the overexpression of the RNA-binding-deficient Zuc mutants retaining residual ssRNase activity (Nishimasu et al., 2012). Thus, we cannot completely rule out the possibility that the ssRNase activity of Mael is required for TE silencing. To fully understand the multiple roles of Mael, an enigmatic key factor in the piRNA pathway, it will be critical to elucidate (1) its ssRNA cleavage mechanism,

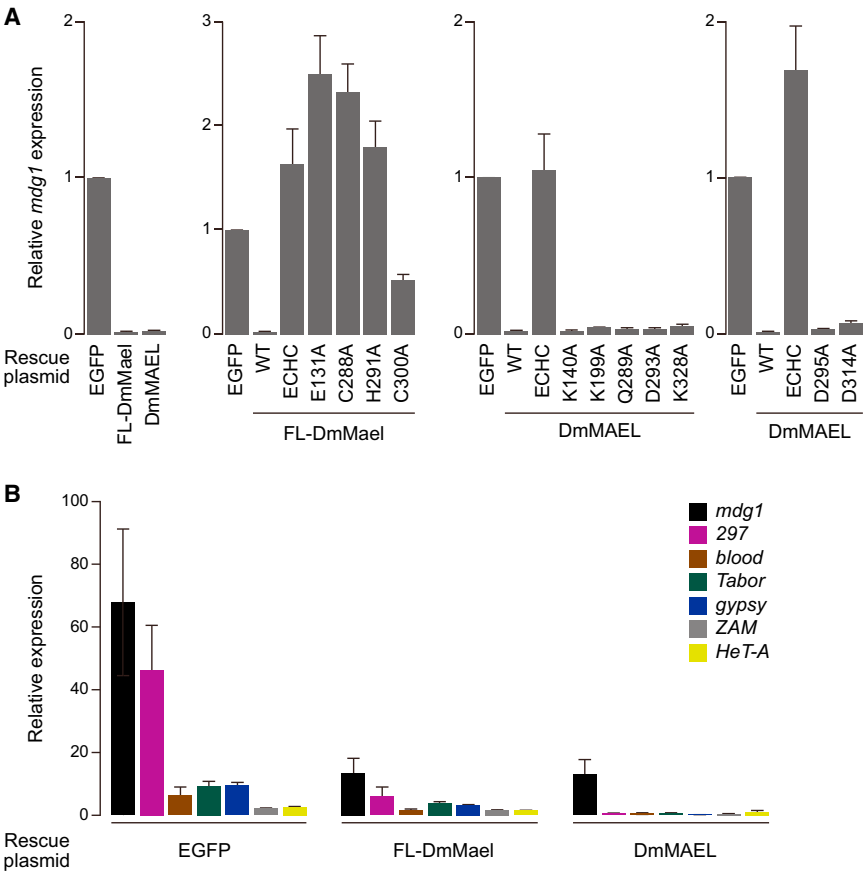

Figure 4. Effects of Mael Mutations on TE Silencing in OSCs

(A) Repression of the *mdg1* transposon by FL-DmMael, DmMAEL, the ECHC-motif mutants of FL-DmMael, the ECHC-motif quadruple mutant of DmMAEL, and the ssRNase-deficient mutants of DmMAEL. Myc-tagged proteins were overexpressed in *mael*-depleted *Drosophila* OSCs, and the expression levels of the *mdg1* transposon were monitored by qRT-PCR (n = 3; error bars indicate SEM). Myc-tagged EGFP was used as a control. The ECHC mutant represents the E131A/C288A/H291A/C300A quadruple mutant.

(B) Repression of a subset of TEs by FL-DmMael and DmMAEL.

See also Figure S4 and Table S2.

(2) its endogenous ssRNA substrates, and (3) the physiological relevance of its ssRNase activity.

EXPERIMENTAL PROCEDURES

Detailed experimental procedures are described in Supplemental Experimental Procedures, and related sequences are shown in Table S2.

DmMAEL (residues 84–333, C228S) was expressed in *E. coli* as a His-tagged protein, and purified by chromatography on Ni-NTA Superflow (QIAGEN) and Resource Q (GE Healthcare) columns. Crystals were obtained at 20°C by the sitting-drop vapor diffusion method. X-ray diffraction data were collected on beamline BL32XU at SPring-8 (Hyogo). The crystal structure of DmMAEL was determined by the SAD method, using the intrinsic zinc atom.

For nuclease activity measurements, the wild-type and mutants of DmMAEL and BmMAEL (residues 92–335) were expressed in *E. coli* as His-tagged proteins, and the proteins were purified by chromatography on Ni-NTA Superflow, Resource Q, Resource PHE (GE Healthcare), and Superdex 200 10/300 (GE Healthcare) columns. MmMAEL (residues 83–327) was expressed in Sf9 insect cells as a His-SUMOstar-tagged protein (LifeSensors) and purified by chromatography using a similar protocol as for DmMAEL. Nuclease activity measurements were performed in buffer containing 25 mM HEPES-KOH (pH 7.4) and 5 mM DTT. Rescue experiments were performed essentially as described previously (Nishimasu et al., 2012).

ACCESSION NUMBERS

The atomic coordinates of DmMAEL have been deposited in the Protein Data Bank under accession number 4YBG. The sequencing data of *Bombyx mori* Mael have been deposited in GenBank under accession number LC032360.

SUPPLEMENTAL INFORMATION

Supplemental Information includes Supplemental Experimental Procedures, four figures, and two tables and can be found with this article online at http://dx.doi.org/10.1016/j.celrep.2015.03.030.

AUTHOR CONTRIBUTIONS

N.M., K.S., H.S., H.N., M.C.S., and O.N. designed the experiments; N.M., R.I., and H.N. performed the structural analysis; N.M. performed the nuclease activity measurement; K.S., Y.N. and K.M. performed the cell-based analysis; N.D. performed the mass spectrometric analysis; N.M., K.S., H.N., M.C.S., and O.N. wrote the manuscript; and all authors discussed the data and the manuscript. H.N., M.C.S., and O.N. supervised all of the work.

ACKNOWLEDGMENTS

We thank Arisa Kurabayashi for technical assistance, Tomoya Tsukazaki and Kaoru Kumazaki for assistance with data collection, and the beamline staff at BL32XU of SPring-8 for technical assistance during data collection. The X-ray diffraction experiments were performed at BL32XU of SPring-8 (proposal no. 2011B1280). This work was supported by a grant from the Target Protein Research Program (TPRP) from the Ministry of Education, Culture, Sports, Science and Technology (MEXT) (to O.N.), by a grant from the Core Research for Evolutional Science and Technology (CREST) Program, The Creation of Basic Chronic Inflammation from Japan Science and Technology Agency (JST) (to

O.N.), and by a Grant-in-Aid for Scientific Research from MEXT (to H.N. and M.C.S.).

Received: October 17, 2014
Revised: February 19, 2015
Accepted: March 10, 2015
Published: April 9, 2015

REFERENCES

Aravin, A.A., van der Heijden, G.W., Castañeda, J., Vagin, V.V., Hannon, G.J., and Bortvin, A. (2009). Cytoplasmic compartmentalization of the fetal piRNA pathway in mice. PLoS Genet. *5*, e1000764.

Brennecke, J., Aravin, A.A., Stark, A., Dus, M., Kellis, M., Sachidanandam, R., and Hannon, G.J. (2007). Discrete small RNA-generating loci as master regulators of transposon activity in Drosophila. Cell *128*, 1089–1103.

Castañeda, J., Genzor, P., van der Heijden, G.W., Sarkeshik, A., Yates, J.R., 3rd, Ingolia, N.T., and Bortvin, A. (2014). Reduced pachytene piRNAs and translation underlie spermiogenic arrest in Maelstrom mutant mice. EMBO J. *33*, 1999–2019.

Clegg, N.J., Frost, D.M., Larkin, M.K., Subrahmanyan, L., Bryant, Z., and Ruohola-Baker, H. (1997). maelstrom is required for an early step in the establishment of Drosophila oocyte polarity: posterior localization of grk mRNA. Development *124*, 4661–4671.

Clegg, N.J., Findley, S.D., Mahowald, A.P., and Ruohola-Baker, H. (2001). Maelstrom is required to position the MTOC in stage 2-6 Drosophila oocytes. Dev. Genes Evol. *211*, 44–48.

Costa, Y., Speed, R.M., Gautier, P., Semple, C.A., Maratou, K., Turner, J.M.A., and Cooke, H.J. (2006). Mouse MAELSTROM: the link between meiotic silencing of unsynapsed chromatin and microRNA pathway? Hum. Mol. Genet. *15*, 2324–2334.

Czech, B., Preall, J.B., McGinn, J., and Hannon, G.J. (2013). A transcriptome-wide RNAi screen in the Drosophila ovary reveals factors of the germline piRNA pathway. Mol. Cell *50*, 749–761.

Dönertas, D., Sienski, G., and Brennecke, J. (2013). Drosophila Gtsf1 is an essential component of the Piwi-mediated transcriptional silencing complex. Genes Dev. *27*, 1693–1705.

Findley, S.D., Tamanaha, M., Clegg, N.J., and Ruohola-Baker, H. (2003). Maelstrom, a Drosophila spindle-class gene, encodes a protein that colocalizes with Vasa and RDE1/AGO1 homolog, Aubergine, in nuage. Development *130*, 859–871.

Gunawardane, L.S., Saito, K., Nishida, K.M., Miyoshi, K., Kawamura, Y., Nagami, T., Siomi, H., and Siomi, M.C. (2007). A slicer-mediated mechanism for repeat-associated siRNA 5′ end formation in Drosophila. Science *315*, 1587–1590.

Handler, D., Meixner, K., Pizka, M., Lauss, K., Schmied, C., Gruber, F.S., and Brennecke, J. (2013). The genetic makeup of the Drosophila piRNA pathway. Mol. Cell *50*, 762–777.

Hastie, K.M., Kimberlin, C.R., Zandonatti, M.A., MacRae, I.J., and Saphire, E.O. (2011). Structure of the Lassa virus nucleoprotein reveals a dsRNA-specific 3′ to 5′ exonuclease activity essential for immune suppression. Proc. Natl. Acad. Sci. USA *108*, 2396–2401.

Hastie, K.M., King, L.B., Zandonatti, M.A., and Saphire, E.O. (2012). Structural basis for the dsRNA specificity of the Lassa virus NP exonuclease. PLoS ONE *7*, e44211.

Holm, L., and Rosenström, P. (2010). Dali server: conservation mapping in 3D. Nucleic Acids Res. *38*, W545–W549.

Ipsaro, J.J., Haase, A.D., Knott, S.R., Joshua-Tor, L., and Hannon, G.J. (2012). The structural biochemistry of Zucchini implicates it as a nuclease in piRNA biogenesis. Nature *491*, 279–283.

Ishizu, H., Siomi, H., and Siomi, M.C. (2012). Biology of PIWI-interacting RNAs: new insights into biogenesis and function inside and outside of germlines. Genes Dev. *26*, 2361–2373.

Jiang, X., Huang, Q., Wang, W., Dong, H., Ly, H., Liang, Y., and Dong, C. (2013). Structures of arenaviral nucleoproteins with triphosphate dsRNA reveal a unique mechanism of immune suppression. J. Biol. Chem. *288*, 16949–16959.

Le Thomas, A., Rogers, A.K., Webster, A., Marinov, G.K., Liao, S.E., Perkins, E.M., Hur, J.K., Aravin, A.A., and Tóth, K.F. (2013). Piwi induces piRNA-guided transcriptional silencing and establishment of a repressive chromatin state. Genes Dev. *27*, 390–399.

Li, C., Vagin, V.V., Lee, S., Xu, J., Ma, S., Xi, H., Seitz, H., Horwich, M.D., Syrzycka, M., Honda, B.M., et al. (2009). Collapse of germline piRNAs in the absence of Argonaute3 reveals somatic piRNAs in flies. Cell *137*, 509–521.

Lim, A.K., and Kai, T. (2007). Unique germ-line organelle, nuage, functions to repress selfish genetic elements in Drosophila melanogaster. Proc. Natl. Acad. Sci. USA *104*, 6714–6719.

Luteijn, M.J., and Ketting, R.F. (2013). PIWI-interacting RNAs: from generation to transgenerational epigenetics. Nat. Rev. Genet. *14*, 523–534.

Majorek, K.A., Dunin-Horkawicz, S., Steczkiewicz, K., Muszewska, A., Nowotny, M., Ginalski, K., and Bujnicki, J.M. (2014). The RNase H-like superfamily: new members, comparative structural analysis and evolutionary classification. Nucleic Acids Res. *42*, 4160–4179.

Malone, C.D., and Hannon, G.J. (2009). Small RNAs as guardians of the genome. Cell *136*, 656–668.

Malone, C.D., Brennecke, J., Dus, M., Stark, A., McCombie, W.R., Sachidanandam, R., and Hannon, G.J. (2009). Specialized piRNA pathways act in germline and somatic tissues of the Drosophila ovary. Cell *137*, 522–535.

Martínez-Sobrido, L., Giannakas, P., Cubitt, B., García-Sastre, A., and de la Torre, J.C. (2007). Differential inhibition of type I interferon induction by arenavirus nucleoproteins. J. Virol. *81*, 12696–12703.

Muerdter, F., Guzzardo, P.M., Gillis, J., Luo, Y., Yu, Y., Chen, C., Fekete, R., and Hannon, G.J. (2013). A genome-wide RNAi screen draws a genetic framework for transposon control and primary piRNA biogenesis in Drosophila. Mol. Cell *50*, 736–748.

Niki, Y., Yamaguchi, T., and Mahowald, A.P. (2006). Establishment of stable cell lines of Drosophila germ-line stem cells. Proc. Natl. Acad. Sci. USA *103*, 16325–16330.

Nishimasu, H., Ishizu, H., Saito, K., Fukuhara, S., Kamatani, M.K., Bonnefond, L., Matsumoto, N., Nishizawa, T., Nakanaga, K., Aoki, J., et al. (2012). Structure and function of Zucchini endoribonuclease in piRNA biogenesis. Nature *491*, 284–287.

Ohtani, H., Iwasaki, Y.W., Shibuya, A., Siomi, H., Siomi, M.C., and Saito, K. (2013). DmGTSF1 is necessary for Piwi-piRISC-mediated transcriptional transposon silencing in the Drosophila ovary. Genes Dev. *27*, 1656–1661.

Olivieri, D., Sykora, M.M., Sachidanandam, R., Mechtler, K., and Brennecke, J. (2010). An in vivo RNAi assay identifies major genetic and cellular requirements for primary piRNA biogenesis in Drosophila. EMBO J. *29*, 3301–3317.

Pace, C.N., Heinemann, U., Hahn, U., and Saenger, W. (1991). Ribonuclease T1: structure, function, and stability. Angew. Chem. Int.Ed. Engl. *30*, 343–360.

Pek, J.W., Lim, A.K., and Kai, T. (2009). Drosophila maelstrom ensures proper germline stem cell lineage differentiation by repressing microRNA-7. Dev. Cell *17*, 417–424.

Pek, J.W., Ng, B.F., and Kai, T. (2012). Polo-mediated phosphorylation of Maelstrom regulates oocyte determination during oogenesis in Drosophila. Development *139*, 4505–4513.

Qi, X., Lan, S., Wang, W., Schelde, L.M., Dong, H., Wallat, G.D., Ly, H., Liang, Y., and Dong, C. (2010). Cap binding and immune evasion revealed by Lassa nucleoprotein structure. Nature *468*, 779–783.

Reuter, M., Berninger, P., Chuma, S., Shah, H., Hosokawa, M., Funaya, C., Antony, C., Sachidanandam, R., and Pillai, R.S. (2011). Miwi catalysis is required for piRNA amplification-independent LINE1 transposon silencing. Nature *480*, 264–267.

Rozhkov, N.V., Hammell, M., and Hannon, G.J. (2013). Multiple roles for Piwi in silencing Drosophila transposons. Genes Dev. *27*, 400–412.

Saito, K., Inagaki, S., Mituyama, T., Kawamura, Y., Ono, Y., Sakota, E., Kotani, H., Asai, K., Siomi, H., and Siomi, M.C. (2009). A regulatory circuit for piwi by the large Maf gene traffic jam in Drosophila. Nature *461*, 1296–1299.

Saito, K., Ishizu, H., Komai, M., Kotani, H., Kawamura, Y., Nishida, K.M., Siomi, H., and Siomi, M.C. (2010). Roles for the Yb body components Armitage and Yb in primary piRNA biogenesis in Drosophila. Genes Dev. *24*, 2493–2498.

Sato, K., Nishida, K.M., Shibuya, A., Siomi, M.C., and Siomi, H. (2011). Maelstrom coordinates microtubule organization during Drosophila oogenesis through interaction with components of the MTOC. Genes Dev. *25*, 2361–2373.

Sienski, G., Dönertas, D., and Brennecke, J. (2012). Transcriptional silencing of transposons by Piwi and maelstrom and its impact on chromatin state and gene expression. Cell *151*, 964–980.

Siomi, M.C., Sato, K., Pezic, D., and Aravin, A.A. (2011). PIWI-interacting small RNAs: the vanguard of genome defence. Nat. Rev. Mol. Cell Biol. *12*, 246–258.

Soper, S.F.C., van der Heijden, G.W., Hardiman, T.C., Goodheart, M., Martin, S.L., de Boer, P., and Bortvin, A. (2008). Mouse maelstrom, a component of nuage, is essential for spermatogenesis and transposon repression in meiosis. Dev. Cell *15*, 285–297.

Wang, S.H., and Elgin, S.C.R. (2011). Drosophila Piwi functions downstream of piRNA production mediating a chromatin-based transposon silencing mechanism in female germ line. Proc. Natl. Acad. Sci. USA *108*, 21164–21169.

Zhang, D., Xiong, H., Shan, J., Xia, X., and Trudeau, V.L. (2008). Functional insight into Maelstrom in the germline piRNA pathway: a unique domain homologous to the DnaQ-H 3′-5′ exonuclease, its lineage-specific expansion/loss and evolutionarily active site switch. Biol. Direct *3*, 48.

Zuo, Y., and Deutscher, M.P. (2001). Exoribonuclease superfamilies: structural analysis and phylogenetic distribution. Nucleic Acids Res. *29*, 1017–1026.

Cell Reports

Supplemental Information

Crystal Structure and Activity of the Endoribonuclease Domain of the piRNA Pathway Factor Maelstrom

Naoki Matsumoto, Kaoru Sato, Hiroshi Nishimasu, Yurika Namba, Kana Miyakubi, Naoshi Dohmae, Ryuichiro Ishitani, Haruhiko Siomi, Mikiko C. Siomi, and Osamu Nureki

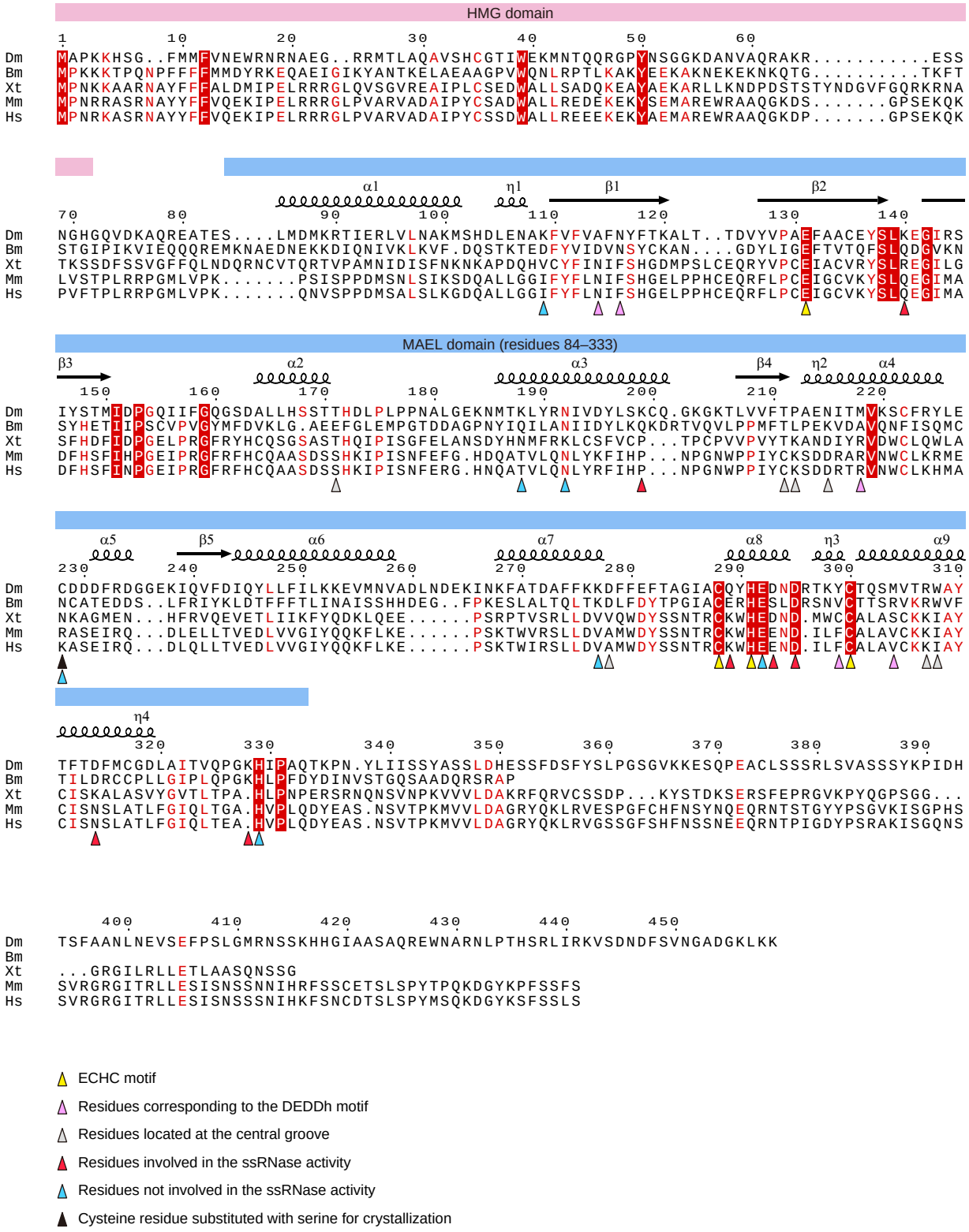

Figure S1. Multiple amino acid sequence alignment of Mael orthologs from higher eukaryotes, Related to Figure 1

Multiple sequence alignment of Mael orthologs from *Drosophila melanogaster* (Dm), *Bombyx mori* (Bm), *Xenopus tropicalis* (Xt), *Mus musculus* (Mm) and *Homo sapiens* (Hs). The secondary structure of DmMAEL is indicated above the sequences. The ECHC-motif residues are indicated by yellow triangles. Residues equivalent to the DEDDh motif are indicated by pink triangles. Residues at the central groove are indicated by gray triangles. Cys228, which was substituted with serine for crystallization, is indicated by a black triangle. Residues involved in the ssRNase activity are indicated by red triangles, whereas residues not involved in the ssRNase activity are indicated by cyan triangles.

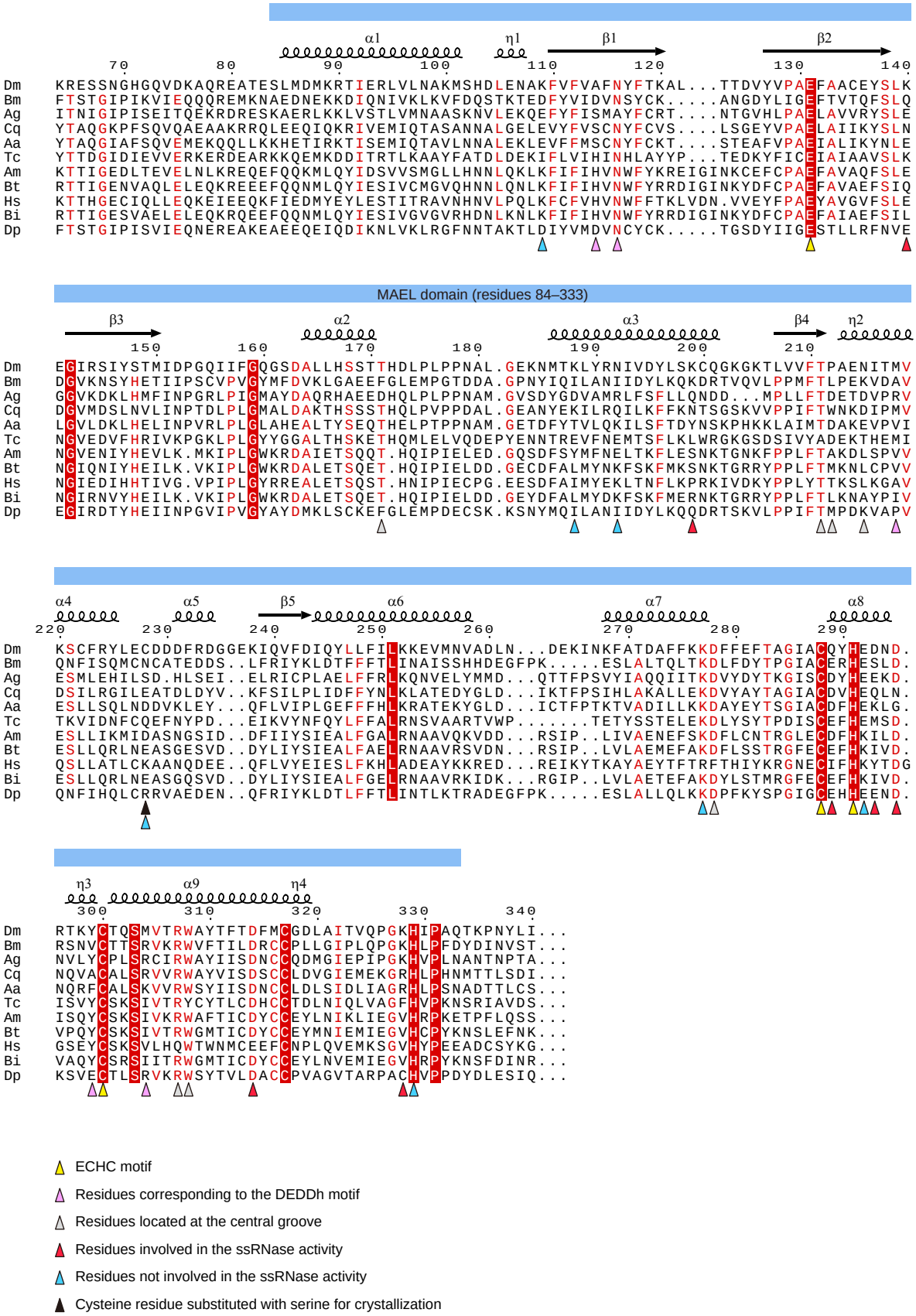

Figure S2. Multiple amino acid sequence alignment of the MAEL domains from insect species, Related to Figure 1

Multiple sequence alignment of the MAEL domains from *Drosophila melanogaster* (Dm), *Bombyx mori* (Bm), *Anopheles gambiae* (Ag), *Culex quinquefasciatus* (Cq), *Aedes aegypti* (Aa), *Tribolium castaneum* (Tc), *Apis mellifera* (Am), *Bombus terrestris* (Bt), *Harpegnathos saltator* (Hs), *Bombus impatiens* (Bi) and *Danaus plexippus* (Dp). The color code of the triangles is the same as in Figure S1.

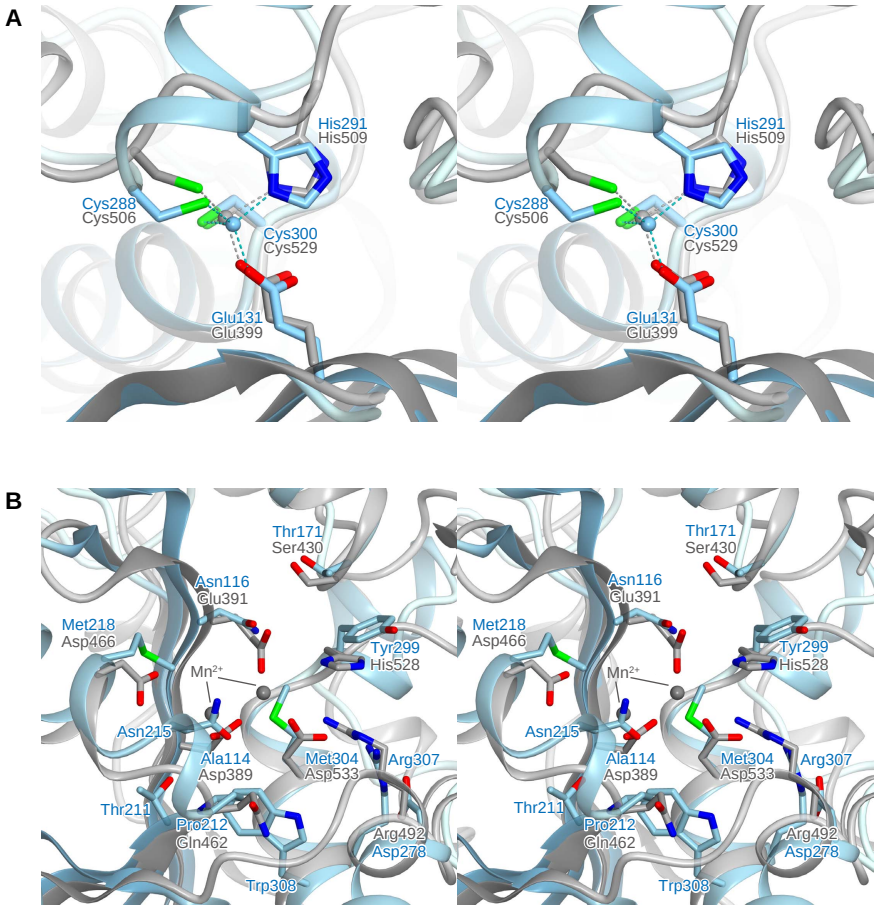

Figure S3. Structural comparison of DmMAEL with LASV NP, Related to Figure 1

(A) Stereo view of the superimposition of the ECHC motifs of DmMAEL (light blue) and LASV NP (gray). The bound zinc ions are shown as spheres.

(B) Stereo view of the superimposition of the central groove of DmMAEL (light blue) and the catalytic groove of LASV NP (gray). The manganese ions bound to LASV NP are shown as gray spheres.

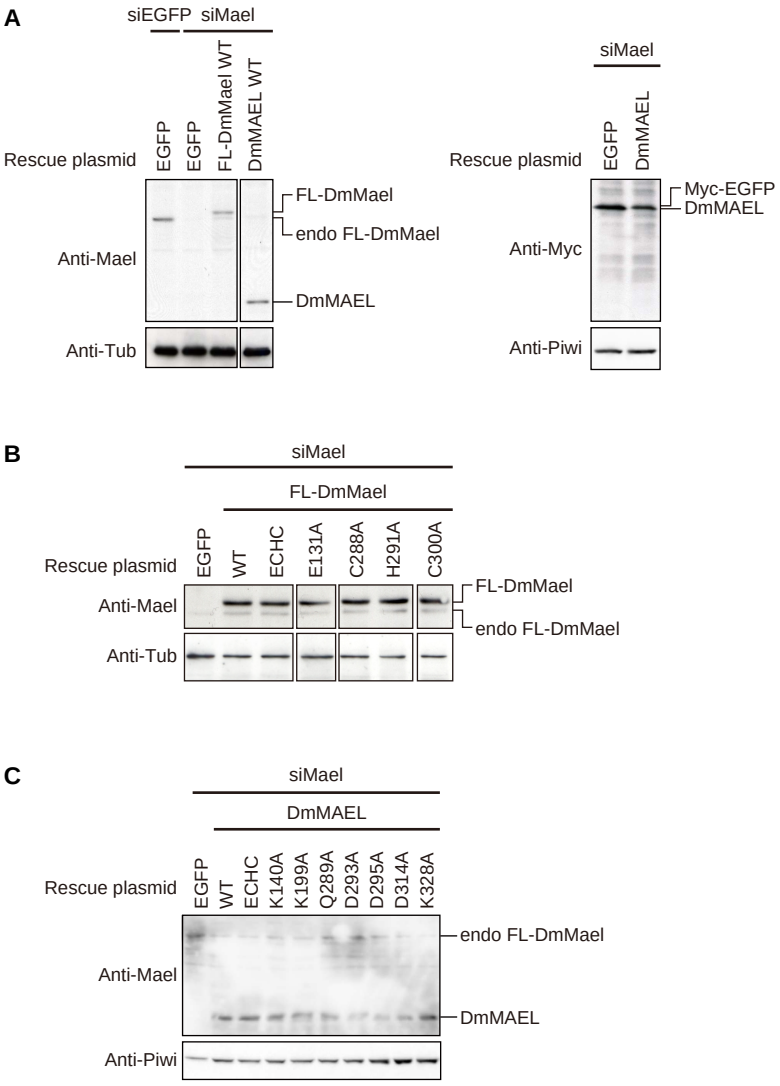

Figure S4. Expression levels of Mael in *Drosophila* OSCs, Related to Figure 4

The expression levels of wild-type FL-DmMael and DmMAEL (A), the ECHC-motif mutants of FL-DmMael (B), the ECHC-motif quadruple mutant and the ssRNase-deficient mutants of DmMAEL (C) were examined by western blotting using an anti-Mael or anti-Myc antibody. Tubulin or Piwi was used as a loading control. WT, wild type.

Table S1. Data Collection and Refinement Statistics, Related to Figure 1

	DmMAEL (Crystal I)	DmMAEL (Crystal II)
Data collection		
Beamline	SPring-8 BL32XU	SPring-8 BL32XU
Wavelength (Å)	1.282	1.000
Space group	$P4_32_12$	$P4_32_12$
Cell dimensions		
a, *b*, *c* (Å)	71.9, 71.9, 86.8	71.9, 71.9, 88.4
α, *β*, *γ* (°)	90, 90, 90	90, 90, 90
Resolution (Å)	50.0–2.40 (2.55–2.40)	50.0–1.60 (1.70–1.60)
R_{sym}	0.157 (0.897)	0.088 (1.17)
$I/\sigma I$	8.13 (2.01)	18.7 (2.40)
Completeness (%)	92.8 (95.3)	99.8 (99.6)
Redundancy	4.08 (3.86)	14.3 (14.3)
CC(1/2)	0.992 (0.715)	0.999 (0.797)
Refinement		
Resolution (Å)		33.4–1.60
No. reflections		31,075
R_{work} / R_{free}		0.194 / 0.216
No. atoms		
Protein		1,902
Ligand		8
Zinc ion		1
Solvent		82
B-factors (Å^2)		
Protein		31.0
Ligand		43.8
Zinc ion		17.9
Solvent		34.4
R.m.s. deviations		
Bond lengths (Å)		0.011
Bond angles (°)		1.289
Ramachandran plot		
Favored (%)		98.3
Allowed (%)		1.7
Outlier (%)		0.0

*Highest resolution shell is shown in parentheses.

Table S2. Oligonucleotide Sequences, Related to Figures 2 and 4

Oligonucleotides for nuclease activity measurement	
40-nt sense RNA	GGUCUGAUUUCGAUCUGGUUCCCUGGAACAAAAGUGGCAG
40-nt antisense RNA	CUGCCACUUUUGUUCCAGGGAACCAGAUCGAAAUCAGACC
40-nt sense DNA	GGTCTGATTTCGATCTGGTTCCCTGGAACAAAAGTGGCAG
40-nt antisense DNA	CTGCCACTTTTGTTCCAGGGAACCAGATCGAAATCAGACC
15-nt poly(A)	AAAAAAAAAAAAAAA
15-nt poly(A) with 1G	AAAAAAAGAAAAAAA
15-nt poly(A) with 3G	AAAAAAGGGAAAAAA
siRNAs for rescue experiment	
siMael sense	CGCCAAGAUGUCCCAUGAUTT
siMael antisense	AUCAUGGGACAUCUUGGCGTT
siEGFP sense	GGCAAGCUGACCCUGAAGUTT
siEGFP antisense	ACUUCAGGGUCAGCUUGCCTT
Primers for qRT-PCR analysis	
*mdg1*_forward	AACAGAAACGCCAGCAACAGC
*mdg1*_reverse	CGTTCCCATGTCCGTTGTGAT
*297*_forward	CTGGCAAAGGGATTTCATCA
*297*_reverse	TGCATTCCTAAGGCCAAATG
*blood*_forward	TATCGCATGGCAGATAGCCAAA
*blood*_reverse	CGTGGAATTCGGAAGTGGTTTC
*Tabor*_forward	ACGTTGTTCACGACATTAGCCG
*Tabor*_reverse	GGGTTGGTTCGGATCTGACG
*gypsy*_forward	ACTAGACTGCACGTACTCGGACA
*gypsy*_reverse	GTTAGCTTCTTTTCAACTTCATCGT
*ZAM*_forward	ACTTGACCTGGATACACTCACAAC
*ZAM*_reverse	GAGTATTACGGCGACTAGGGATAC
*HeT-A*_forward	CGCGCGGAACCCATCTTCAGA
*HeT-A*_reverse	CGCCGCAGTCGTTTGGTGAGT
*rp49*_forward	CCGCTTCAAGGGACAGTATCTG
*rp49*_reverse	ATCTCGCCGCAGTAAACGC
Primers for cloning	
Bm-forward	TTTTTGGTACCATGCCAAAAAAGAAGACCCCACA
Bm-reverse	TTTTTGCGGCCGCAGGGTGCTCTGGACCTTTG
Mm-forward	TTTTTGGATCCCCATGCCCAACCGCAGGGCC
Mm-reverse	TTTTTGTCGACTTAAGAAAAGGAGGAGAAAGG

SUPPLEMENTAL EXPERIMENTAL PROCEDURES

Protein preparation

The gene encoding *D. melanogaster* Mael (residues 1–459, referred to as FL-DmMael) was amplified by PCR using pBlueScript-FL-DmMael (Sato et al., 2011) as the template. The PCR product was cloned between the *Nde*I and *Xho*I sites of a modified pET28a vector (Novagen), in which the thrombin protease recognition sequence was replaced with the Turbo3C Protease recognition site. FL-DmMael was expressed in *E. coli* Rosetta2 (DE3) cells (Novagen), and was purified by chromatography on Ni-NTA Superflow (QIAGEN), Resource Q (GE Healthcare) and Superdex 200 10/300 (GE Healthcare) columns. We only obtained a small amount of purified FL-DmMael (0.03 mg from 1 liter *E. coli* culture), due to its low expression levels. To identify a well-expressed, stable region suitable for structural and biochemical studies, we performed limited proteolysis experiments. Purified FL-DmMael was digested with trypsin (Sigma) (20:1, w/w) at 26°C for 20 min, and the products were resolved by 12% sodium dodecyl sulfate polyacrylamide gel electrophoresis (SDS-PAGE), followed by N-terminal amino acid and mass spectrometric analyses. The limited proteolysis experiments revealed that the MAEL domain of *D. melanogaster* Mael (residues 84–333, referred to as DmMAEL) is a stable 28 kDa fragment.

The gene encoding DmMAEL was cloned between the *Nde*I and *Xho*I sites of the modified pET28a vector, and DmMAEL was overexpressed as an N-terminal His-tagged protein in *E. coli* Rosetta2 (DE3) cells. The *E. coli* cells harboring the expression plasmid were cultured at 37°C in LB medium, containing 50 mg l^{-1} kanamycin. Protein expression was induced by the addition of 0.1 mM isopropyl-β-D-thiogalactopyranoside, when the culture reached an OD_{600} of 0.8. The *E. coli* cells were further cultured at 15°C for 18 h, and were harvested by centrifugation. The *E. coli* cells were resuspended in buffer (50 mM Tris-HCl, pH 8.0, 300 mM NaCl, 20 mM imidazole, 3 mM 2-mercaptoethanol, 5% glycerol), lysed by sonication, and centrifuged. The supernatant was incubated with 3 ml Ni-NTA Superflow resin, and the mixture was then loaded into an Econo-Column (Bio-Rad). The protein was eluted with buffer (20 mM Tris-HCl, pH 8.0, 300 mM NaCl, 300 mM imidazole, 3 mM 2-mercaptoethanol, 5% glycerol). The eluted protein was treated with Turbo3C Protease (Nacalai Tesque) at 4°C for 16 h to cleave the N-terminal His tag, and then was passed through the Ni-NTA column again. The protein was loaded onto a Resource Q column, equilibrated with buffer (20 mM Tris-HCl, pH 8.0, 30 mM NaCl, 1 mM DTT), and was eluted using a linear gradient of 30–600 mM NaCl. The purified protein was dialyzed against buffer (10 mM Tris-HCl, pH 8.0, 150 mM NaCl, 1 mM DTT), and was concentrated to 5 mg ml^{-1} using an Amicon Ultra 10K filter (Millipore).

DmMAEL generated crystals under several conditions, but the crystals diffracted poorly. We thus prepared the five less-conserved cysteine mutants (C135V, C200S, C222S, C228S and C317A), using a PCR-based method. The sequences were verified by DNA sequencing. All of the cysteine mutants were expressed in *E. coli*, and were purified by a protocol similar to that for wild-type DmMAEL.

Crystallization

Crystallization was performed at 20°C, using the sitting-drop vapor diffusion method. Of the five cysteine mutants, only the DmMAEL C228S mutant generated well-diffracting crystals. We obtained crystals of the DmMAEL C228S mutant (Crystal I), by mixing 0.1 µl of protein solution (5 mg ml^{-1} DmMAEL, 10 mM Tris-HCl, pH 8.0, 150 mM NaCl, 1 mM DTT) and 0.1 µl of reservoir solution (200 mM ammonium acetate, 20% PEG3350). Furthermore, we obtained better-diffracting crystals (Crystal II) by the streak-seeding technique, using a slightly different reservoir solution (200 mM ammonium acetate, 19% PEG3350).

Data collection, structure determination and refinement

Crystals were cryoprotected by the reservoir solution supplemented with 25% ethylene glycol. X-ray diffraction data sets were collected at 100 K, on the beamline BL32XU at SPring-8 (Hyogo, Japan). Diffraction data were processed using XDS (Kabsch, 2010). We performed zinc K-edge X-ray absorption fine structure experiments, and found that the crystal contains endogenous zinc atoms. Diffraction data sets for Crystal I (2.4 Å resolution) and Crystal II (1.6 Å resolution) were collected at wavelengths of 1.282 Å and 1.000 Å, respectively. The crystal structure of DmMAEL was determined by the SAD method, using the 2.4 Å resolution data set from Crystal I. One zinc site was located by the program SHELXD (Sheldrick, 2008), and the experimental phases were calculated with the program SHARP (Bricogne et al., 2003). The atomic model was automatically built with the program RESOLVE (Terwilliger, 2003). The resultant model

was manually built with the program COOT (Emsley et al., 2010), and refined with the program PHENIX (Adams et al., 2002). The final model was refined at 1.6 Å resolution, with R_{work}/R_{free} of 19.4%/21.6%, using the data set from Crystal II. A summary of the crystallographic data collection and refinement statistics is provided in Table S1. Structural figures were prepared with the program CueMol (http://www.cuemol.org).

Nuclease activity measurement

The gene encoding *B. mori* Mael (residues 1–354) was amplified by RT-PCR from total RNA from *B. mori* ovary-derived BmN4 cells, and cloned into the pGEX-5X-1 vector (GE Healthcare). Using this vector as the template, the expression plasmid encoding the MAEL domain of *B. mori* Mael (residues 92–335, referred to as BmMAEL) was prepared in a similar manner as described for DmMAEL. The wild type and mutants of DmMAEL and BmMAEL were expressed in *E. coli*, and the proteins were purified by chromatography on Ni-NTA Superflow and Resource Q columns, using a protocol similar to that for DmMAEL. To avoid the potential cleavage of nucleic acid substrates by contaminants from *E. coli*, the proteins were further purified by chromatography on Resource PHE (GE Healthcare) and Superdex 200 10/300 (GE Healthcare) columns. The gene encoding *M. musculus* Mael (residues 1–434) was amplified by RT-PCR from total RNA from C57BL/6J line mouse testis (Japan SLC, Inc), and cloned into the pGEX-5X-1 vector. Using this vector as the template, the expression plasmid encoding the MAEL domain of *M. musculus* Mael (residues 83–327, referred to as MmMAEL) was amplified by PCR, and the PCR product was cloned into a modified pFastBac HTa vector (Invitrogen), in which the SUMOstar tag (LifeSensors) was inserted between the histidine tag and TEV protease cleavage site. MmMAEL was expressed in Sf9 insect cells. Baculovirus-infected Sf9 cells were cultured in Sf900II (Invitrogen) at 27°C, and were harvested 60 h after infection by centrifugation. The insect cells were resuspended in buffer (20 mM phosphate buffer, pH 7.3, 300 mM NaCl, 20 mM imidazole, 3 mM 2-mercaptoethanol, 5% glycerol, 1 mM phenylmethylsulfonyl fluoride), lysed by sonication, and ultracentrifuged. The supernatant was incubated with Ni-NTA Superflow resin, and MmMAEL was eluted with buffer (20 mM phosphate buffer, pH 7.3, 300 mM NaCl, 300 mM imidazole, 3 mM 2-mercaptoethanol, 5% glycerol, 1 mM phenylmethylsulfonyl fluoride). The eluted protein was treated with TEV protease at 4°C for 16 h to cleave the N-terminal His-SUMOstar tag, and was passed through the Ni-NTA column again. The protein was further purified by chromatography on Resource Q, Resource PHE and Superdex 200 10/300 columns, using a protocol similar to those for DmMAEL and BmMAEL. The purified proteins were analyzed by 15% SDS-PAGE, and stained with SimplyBlue Safestain (Invitrogen).

The nucleic acid substrates used for the activity measurements are listed in Table S2. The ssRNAs and ssDNAs were purchased from GeneDesign and Eurofins Genomics, respectively. The ssRNAs and ssDNAs were 5′-radiolabeled with ^{32}P-γ-ATP and T4 polynucleotide kinase (New England Biolabs), and were purified by 15% denaturing (6 M urea) PAGE. To prepare the dsRNA and dsDNA substrates, the radiolabeled antisense strands were mixed with a 2-fold excess of the non-labeled, complementary sense strands in buffer (10 mM Tris-HCl, pH 7.5, 50 mM NaCl, 1 mM EDTA), heated at 95°C for 15 min, and then gradually cooled to 30°C. To prepare the circular ssRNA substrate, the radiolabeled ssRNA was incubated at 37°C for 15 min with ATP and T4 RNA ligase 1 (New England Biolabs) in buffer (50 mM Tris-HCl, pH 7.8, 10 mM $MgCl_2$, 1 mM DTT), and then purified by 10% denaturing (6 M urea) PAGE. Prior to the cleavage reactions, all of the radiolabeled single-stranded substrates were unfolded by an incubation at 95°C for 2 min, followed by immediate cool down at 4°C.

The purified DmMAEL (2.2 μM) was incubated with substrates (10^4 c.p.m.) at 26°C for 3 h, in 20 μl of reaction buffer (25 mM HEPES-KOH, pH 7.4, 5 mM DTT). The reaction mixture was mixed with an equal volume of loading buffer (98% w/v deionized formamide, 10 mM EDTA, pH 8.0, 0.025% w/v xylene cyanol, 0.025% w/v bromophenol blue), heated at 95°C for 2 min, and then analyzed by 15% denaturing (6 M urea) PAGE. The radioactive signals were detected using a Typhoon FLA 9500 image analyzer (GE Healthcare). The effects of $MgCl_2$ and $CaCl_2$ on the nuclease activity were examined using reaction buffers (25 mM HEPES-KOH, pH 7.4, 5 mM DTT, 3 mM $MgCl_2$ or $CaCl_2$). The effects of NaCl were examined using reaction buffers (25 mM HEPES-KOH, pH 7.4, 5 mM DTT, 0–100 mM NaCl). Exonuclease T (7.5 units) (New England Biolabs) was incubated with the circular ssRNA in reaction buffer (50 mM potassium acetate, 20 mM Tris-acetate, pH 7.9, 10 mM magnesium acetate, 1 mM DTT). The effects of the substrate structure on the nuclease activity were examined using 15-nt poly(A) containing 0, 1 or 3 guanine residues. To compare the enzymatic properties of DmMAEL and RNase T1, the ssRNase activities of DmMAEL (0.14–2.2 μM) and RNase T1 (Ambion) (0.5–10 units) were measured using the 40AS ssRNA as the

substrate. The ssRNase activities of DmMAEL (1 μM) and BmMAEL (1 μM) were measured at 26°C for 3 h, and that of MmMAEL (1 μM) was measured at 37°C for 3 h, using the 40AS ssRNA as the substrate. To identify the residues involved in ssRNA cleavage, the ssRNase activities of the wild type and mutants of DmMAEL (1 μM) were measured at 26°C for 1 h, using the 40AS ssRNA as the substrate.

Rescue experiments in OSCs

The gene encoding FL-DmMael was amplified by RT-PCR from total RNA from *Drosophila* ovary, and was cloned between the *Kpn*I and *Xho*I sites of the pAcM vector (Saito et al., 2010). The rescue plasmids encoding the RNAi-resistant, wild type and mutants of FL-DmMael were prepared by a PCR-based method, using pAcM-FL-DmMael as the template. The rescue plasmids encoding the wild type and mutants of DmMAEL were prepared by a PCR-based method, using pAcM-FL-DmMael as the template. pAcM-EGFP was used as a negative control (Saito et al., 2010).

Transfection was performed essentially as described previously (Saito et al., 2010). Briefly, trypsinized OSCs (3×10^6 cells) were transfected with the siRNA duplex (300 pmol) and rescue plasmid (5 μg) using Nucleofector (Lonza), and then transferred to fresh OSC medium. After an incubation at 26°C for 2 days, total RNA was purified using the ISOGEN reagent (Nippon Gene) or the RNAzol RT reagent (Cosmo Bio). cDNAs were synthesized from 1 μg total RNA, using a Transcriptor First Strand cDNA Synthesis Kit (Roche Diagnostics) and an oligo(dT) primer. qRT-PCR was performed with SYBR Premix Ex Taq (Takara) or THUNDERBIRD SYBR qPCR Mix (TOYOBO), using a LightCycler Real-Time PCR system (Roche Diagnostics) or a StepOnePlus system (Applied Biosystems). The amplification efficiency of the qRT-PCR was calculated, based on the slope of the standard curve. After confirmation of the amplification efficiency values (between 95% and 105%), the relative steady-state mRNA levels were determined from the threshold cycle for the amplification, using *ribosomal protein 49* (*rp49*) as an internal control. The expression levels of DmMael, Piwi and tubulin were analyzed by western blotting, using the culture supernatants of anti-Mael hybridoma cells (Sato et al., 2011), anti-Piwi hybridoma cells (Saito et al., 2006), and an anti-tubulin antibody (Developmental Studies Hybridoma Bank, E7), respectively. The siRNA duplexes and the qRT-PCR primers are listed in Table S2.

SUPPLEMENTAL REFERENCES

Adams, P.D., Grosse-Kunstleve, R.W., Hung, L.W., Ioerger, T.R., McCoy, A.J., Moriarty, N.W., Read, R.J., Sacchettini, J.C., Sauter, N.K., and Terwilliger, T.C. (2002). PHENIX : building new software for automated crystallographic structure determination. Acta Crystallogr. D Biol. Crystallogr. *58*, 1948–1954.

Bricogne, G., Vonrhein, C., Flensburg, C., Schiltz, M., and Paciorek, W. (2003). Generation, representation and flow of phase information in structure determination: recent developments in and around SHARP 2.0. Acta Crystallogr. D Biol. Crystallogr. *59*, 2023–2030.

Emsley, P., Lohkamp, B., Scott, W.G., and Cowtan, K. (2010). Features and development of Coot. Acta Crystallogr. D. Biol. Crystallogr. *66*, 486–501.

Kabsch, W. (2010). Xds. Acta Crystallogr. D Biol. Crystallogr. *66*. 125–132.

Saito, K., Nishida, K.M., Mori, T., Kawamura, Y., Miyoshi, K., Nagami, T., Siomi, H., and Siomi, M.C. (2006). Specific association of Piwi with rasiRNAs derived from retrotransposon and heterochromatic regions in the Drosophila genome. Genes Dev. *20*, 2214–2222.

Sheldrick, G.M. (2008). A short history of SHELX. Acta Crystallogr. A. *64*, 112–122.

Terwilliger, T.C. (2003). Automated main-chain model building by template matching and iterative fragment extension. Acta Crystallogr. D Biol. Crystallogr. *59*, 38–44.